

# Periodic ground state for the charged massive Schwinger model

S. Nagy<sup>1</sup>, J. Polonyi<sup>2,3</sup>, and K. Sailer<sup>1</sup>

<sup>1</sup> Department for Theoretical Physics, University of Debrecen, Debrecen, Hungary

<sup>2</sup> Institute for Theoretical Physics, Louis Pasteur University, Strasbourg, France

<sup>3</sup> Department of Atomic Physics, Lorand Eötvös University, Budapest, Hungary

(December 2, 2024)

It is shown by minimizing the tree-level energy density of the bosonised charged massive Schwinger model that the vacuum exhibits a periodic structure for arbitrary values of the charge density. A similar result is obtained in the framework of the fermionic formalism by minimizing the energy with respect to the parameters of an assumed periodic background electric field. The existence of the periodic vacuum obtained numerically for small charge densities has been found also valid for large charge densities by simple analytic calculations in both cases.

12.20.Ds

## I. INTRODUCTION

There are few field theoretical models which are exactly solvable and can be regarded as simple toy models. They have little importance for the real world but may become good testing ground for certain new developments owing to their simplicity. As an example, certain aspects of the confining features of QCD can be investigated in two-dimensional quantum electrodynamics (QED<sub>1+1</sub>), in the Schwinger model [1–4]. The massless Schwinger model [5] is exactly solvable [6] and the explicit computation of the fermion determinant leads to an effective theory with massive photons and confinement [2]. When the vacuum polarization effects are neglected then the electric flux conservation induces a flux tube between an electron-positron pair in the absence of other charges. The resulting linear potential, the hard confinement mechanism, renders the positronium confined. Let us now allow the vacuum polarization to be present and try to separate a member of the positronium, that of the meson of the Schwinger model. The electric flux tube breaks up due to electron-positron pair creation when the energy of the stretched flux tube is sufficiently large and the members of the newly created pair bind to those of the original pair. This is the soft confinement mechanism and one ends up with more neutral mesons again in this manner. The linear potential between the electron-positron pair becomes saturated by virtual pair creations. The potential between a pair of static test charges can easily be obtained in the presence of vacuum polarization [2] and it shows that the total screening, the soft confinement mechanism, occurs for arbitrary value of the charge.

The massive Schwinger model is not exactly solvable and the potential between a pair of test charges is periodic function of the charge with period length given by the elementary charge  $e$  and is saturated for integer multiples of  $e$  only [2]. The mass gap prevents the vacuum to polarize out non-integer multiples of the elementary charge. Notice that the massless model is singular in the sense that arbitrarily small mass is enough to prevent the screening of non-integer charges at sufficiently large distances. At the end any charge is confined in the massive model as well but the integer or non-integer charges are confined by the soft or hard mechanisms, respectively.

Excitations above a fermionic vacuum with well-defined particle number are always consisted of particle-hole pairs and are therefore of bosonic nature. It is the special feature of the 1+1 dimensional world that the effective theory for these bosonic excitations is local. The local effective theory resulting from the bosonisation of the massive Thirring model is the sine-Gordon model [7]. These bosonization rules are widely used for the investigation of the Schwinger model [3,4,8–10]. The massless case yields a free scalar theory and the massive theory leads to the massive sine-Gordon model [11]. The massive Schwinger model was also investigated by bosonization technique [12] and by functional methods [13] at non-vanishing chemical potential  $\mu$  and temperature  $T$ . The existence of a periodic chiral condensate with the wavenumber of  $2\mu$  has been established for arbitrary temperature, too.

Arguments were given in the framework of the tree-level solution of the bosonized model [4] that the massive Schwinger model exhibits a periodic ground state in the presence of a static, homogeneous background charge density, the analogue of the Wigner-crystal [14] in 1+1 dimensions. Another indication of the inhomogeneous vacuum structure comes from the non-relativistic Peierls mechanism [15]. A more systematic investigation of the inhomogeneity of the vacuum of the massive Schwinger model in the presence of homogeneous external charge density,  $\rho_{\text{ext}}$ , is presented in this paper. We attack the problem from two different directions. First by minimizing the tree-level expression of the energy functional in the bosonized form of the model and after that by minimizing the energy with respect to the parameters of a static, periodic background electric field in the fermionic form of the theory and by retaining

the quantum fluctuations of the photon field up to the two-loop order. The results obtained by both approaches are in qualitative agreement. Namely, the ground state exhibits periodically modulated charge density with decreasing amplitude for increasing  $\rho_{\text{ext}}$ . For large  $\rho_{\text{ext}}$  numerical calculations failed to be conclusive regarding the true energy minimum. Analytic considerations were used in this density regime with the result that the vacuum remains periodic for arbitrarily large values of  $\rho_{\text{ext}}$ .

The paper consists of two parts. Section II contains the study of the tree-level bosonized theory in the presence of the homogeneous external charge density  $\rho_{\text{ext}}$ . The minimum of the energy functional of the model is determined by numerical minimization of the classical vacuum energy. For large values of  $\rho_{\text{ext}}$  when the result is more unstable with respect to numerical errors the stability of the periodic vacuum has been shown analytically, by expanding the tree-level energy in powers of the amplitude of charge density wave in the vacuum.

The fermionic investigations are presented in Section III. Since integer charges are screened and do not leave behind long range photon field [4] the perturbation expansion in  $e$  is reliable by using the original fermionic and photonic degrees of freedom. We follow a variational strategy and minimize the energy of the vacuum as the function of the induced photon field in the vacuum. The fermionic degrees of freedom are integrated out in the presence of a static, sinusoidal electric field and the quantum fluctuations of the photon field are taken into account up to two-loop diagrams for the energy. The external charge density  $\rho_{\text{ext}}$  is introduced indirectly via a fermionic chemical potential  $\mu$ . The energy of the vacuum is finally minimized with respect to the amplitude and the wavelength of the static periodic background electric field. The numerical minimization procedure finds the periodic ground state energetically favorable compared to the homogeneous one below certain value of  $\rho_{\text{ext}}$ . The problem of the high density regime is of the same origin as in the bosonized study, namely the smallness of the amplitude of the induced photon field in the vacuum. The energy difference between the homogeneous and the periodically modulated vacuum becomes weak and our errors arising from the truncation of the loop-expansion and the choice of the induced photon field render the computation unreliable.

Finally, the conclusion is drawn up in Sect. IV. Appendix A contains the analytic argument in favor of the inhomogeneous vacuum for large  $\rho_{\text{ext}}$  both for the bosonic and the fermionic formalisms. Appendices B and C present briefly the numerical solutions of the Dirac equation in periodic background potential and the band structure of the fermionic spectrum, respectively. Explicit expressions for the Feynman diagrams up to the two-loop order are given in Appendix D.

## II. MINIMIZATION OF THE ENERGY IN THE BOSONIZED MODEL

This section contains the tree-level determination of the vacuum structure of the bosonized model.

### A. Hamiltonian

The Lagrangean of the massive Schwinger model is given as

$$\mathcal{L} = -\frac{1}{4}F_{\mu\nu}F^{\mu\nu} + \bar{\psi}\gamma^\mu(\partial_\mu - ieA_\mu)\psi - m\bar{\psi}\psi, \quad (1)$$

where  $F_{\mu\nu} = \partial_\mu A_\nu - \partial_\nu A_\mu$ ,  $m$  and  $e$  are the bare rest mass of the electron and the bare coupling constant, respectively. The bosonization rules are [4]:

$$\begin{aligned} :\bar{\psi}\psi: &\rightarrow -cmM\cos(2\sqrt{\pi}\phi), & :\bar{\psi}\gamma_5\psi: &\rightarrow -cmM\sin(2\sqrt{\pi}\phi), \\ j_\mu = :\bar{\psi}\gamma_\mu\psi: &\rightarrow \frac{1}{\sqrt{\pi}}\varepsilon_{\mu\nu}\partial^\nu\phi, & :\bar{\psi}i\partial^\mu\psi: &\rightarrow \frac{1}{2}N_m(\partial_\mu\phi)^2, \end{aligned} \quad (2)$$

where  $N_m$  denotes normal ordering with respect to the fermion mass  $m$ ,  $c = \exp(\gamma)/2\pi$  with the Euler constant  $\gamma$ , and  $M = e/\sqrt{\pi}$  the ‘meson’ mass. It is believed that the presence of a non-vanishing background charge density does not affect these transformation rules [12]. The Hamiltonian of the system in Coulomb gauge is given by

$$\mathcal{H} = \int_x \bar{\psi}_x(i\gamma_1\partial_1 + m)\psi_x - \frac{e^2}{4} \int_{x,y} j_{0,x}|x-y|j_{0,y}, \quad (3)$$

with  $\int_x = \int_0^T dx^0 \int_{-L}^L dx^1$ . According to the bosonization rules this Hamiltonian is equivalent to those of the massive sine-Gordon model,

$$\mathcal{H} = N_m \int_x \left[ \frac{1}{2} \Pi_x^2 + \frac{1}{2} (\partial_1 \phi_x)^2 + \frac{1}{2} M^2 \phi_x^2 - cmM \cos(2\sqrt{\pi} \phi_x) \right] \quad (4)$$

where  $\Pi_x$  denotes the momentum variable canonically conjugated to  $\phi_x$ .

Our purpose is to determine the vacuum of the massive Schwinger model in the presence of an external static charge density  $\rho_{\text{ext } x}$  which is added to the charge density  $j_{0,x}$  in Eq. (3),

$$\mathcal{H} = \int_x \bar{\psi}_x (i\gamma_1 \partial_1 + m) \psi_x - \frac{e^2}{4} \int_{x,y} (j_{0,x} + \rho_{\text{ext } x}) |x - y| (j_{0,y} + \rho_{\text{ext } y}). \quad (5)$$

The external charge is represented by the external field  $\phi_{\text{ext } x}$  in the bosonized Hamiltonian (4) as

$$\mathcal{H} = N_m \int_x \left[ \frac{1}{2} \Pi_x^2 + \frac{1}{2} (\partial_1 \phi_x)^2 + \frac{1}{2} M^2 (\phi_x + \phi_{\text{ext } x})^2 - cmM \cos(2\sqrt{\pi} \phi_x) \right] \quad (6)$$

where

$$\rho_{\text{ext } x} = \frac{1}{\sqrt{\pi}} \partial_1 \phi_{\text{ext } x}. \quad (7)$$

The external charge density is assumed to be static and constant in the interval  $x^1 = z \in [-L, L]$  and vanishing elsewhere, therefore we write  $\phi_{\text{ext } x} = bz$  when  $|z| < L$  and  $\phi_{\text{ext } x} = 0$  elsewhere for any  $x^0 = t$ . The total charge density with this choice of the external field is

$$\rho_x = \frac{1}{\sqrt{\pi}} (\partial_1 \phi_x + bz). \quad (8)$$

The Hamiltonian (4), considered as the functional of the field configuration  $\phi_x$ , gives the tree-level energy. Therefore the field expectation value  $\phi_{\text{gr } x} = \langle 0 | \phi_x | 0 \rangle$  is found in the tree-level approximation by minimizing Eq. (4) in  $\phi_x$  for a given external charge density, i.e. a given value of the parameter  $b$ . The minimum among the static configurations,  $\Pi_x = 0$ , was identified numerically by means of the conjugate gradient method. The tree-level energy,

$$E(b) = \int_z \left[ \frac{1}{2} (\partial_1 \phi_z)^2 + \frac{e^2}{2\pi} (\phi_z + bz)^2 - \frac{cme}{\sqrt{\pi}} \cos(2\sqrt{\pi} \phi_z) \right], \quad (9)$$

has been discretized as

$$E_\Delta(b) = \frac{1}{2\Delta z} \sum_{i=0}^N (\phi_{z_{i+1}} - \phi_{z_i})^2 + \frac{e^2 \Delta z}{2\pi} \sum_{i=0}^N (\phi_{z_i} + bz_i)^2 - \frac{cme \Delta z}{\sqrt{\pi}} \sum_{i=0}^N \cos(2\sqrt{\pi} \phi_{z_i}) \quad (10)$$

with  $z_i = z_0 + i\Delta z$ ,  $\Delta z = 2L/(N+1)$ ,  $z_0 = -L$  and  $z_{N+1} = L$ . The boundary conditions

$$\phi_{z_0} = \phi_{z_{N+1}} = 0 \quad (11)$$

have been used in order to restrict the computation into the sector with vanishing induced charge.

## B. Results

We used  $L = 16\pi$ ,  $N = 800$ ,  $m = 0.5; 2; 5$  and  $b \in [0.3; 7]$  in the numerical work. Iterations of the conjugate gradient method have been started from a number of initial conditions for  $\phi_{z_i}$  and the field configurations corresponding to the lowest energy have been singled out. The charge densities were then calculated according to Eq. (8).

The minimum of the expression (9) was found at  $\phi_z = 0$  for vanishing external charge density, i.e. for  $b = 0$ . The increase of  $b$  gave two distinct regions, separated by a size-dependent point  $b = b_L$ .

$b < b_L$ : For  $b$  close to zero one expects that  $\phi_z$  is small and the sinusoidal potential in the equation of motion,

$$\partial_1 \phi_z = \frac{e^2}{\pi} (\phi_z + bz) + 2cme \sin(2\sqrt{\pi} \phi_z), \quad (12)$$

can well be approximated by the first term of its Taylor series

$$\partial_1 \phi_z \approx \frac{e^2}{\pi} (\phi_z + bz) + 4cme\sqrt{\pi}\phi_z. \quad (13)$$

Such a linearized equation of motion together with the boundary conditions (11) yields

$$\phi_z = b_s L \frac{\sinh(\kappa z)}{\sinh(\kappa L)} - b_s z, \quad \kappa = \sqrt{\frac{e^2}{\pi} + 4cme\sqrt{\pi}}, \quad b_s = b \frac{e^2}{\kappa^2 \pi}. \quad (14)$$

This solution, shown in Fig. 1, contains three spatial regions in the interval  $[-L, L]$  and in the longest, central region  $\phi_z$  is linearly decreasing function with the slope  $-b_s$ . The analytic results for the slope are in very good agreement with those obtained numerically. The linear decrease of  $\phi_z$  in the central region describes the partial screening of the external charge density. In the two other regions, close to the boundaries at  $-L$  and  $L$ ,  $|\phi_z|$  approaches abruptly zero. For every choice of  $L$  a critical  $b_L$  value was found where the linear approximation fails to work and the higher-order terms of the sine function are needed in the equation of motion (12). It was found that the slope  $b_s$  reaches  $b$  at this point. The  $L$ -dependence is  $b_L \approx L^{-1.41}$  according to Fig. 2, therefore  $b_L \rightarrow 0$  and this type of solutions disappears in the thermodynamic limit.

$b_L < b$ : The increase of  $b_s$  to  $b$  indicates the complete screening of the external charge density in the central region. Furthermore the numerical solution, depicted in Fig. 3, reveals an additional periodic structure in  $\phi_z$ . In fact,  $\tilde{\phi}_z$ , introduced by the parametrization  $\phi_z = \tilde{\phi}_z - bz$ , is a periodic function of wavelength  $\ell$ ,  $\tilde{\phi}_z = \tilde{\phi}_{z+\ell}$ . The wavelength  $\ell$  and the amplitude  $A$  of  $\tilde{\phi}_z$  were defined numerically as the distance of the neighbouring zeros of  $\tilde{\phi}_z$  and the arithmetic average of the magnitude  $|\tilde{\phi}_z|$  at the extrema of the periodic component, respectively. Both  $\ell$  and  $A$  decrease with increasing  $b$  in this region as shown in Figs. 4 and 5. The relation  $\ell = 1/\rho_{\text{ext}}$  displayed by Fig. 4 reflects the fact that charges which are integer multiples of  $e$  are completely screened. In fact, as argued in Ref. [4], the introduction of the charges  $\pm e$  at the boundaries corresponds to the shift  $z \rightarrow z + \delta z$  with  $|\delta z| = \sqrt{\pi}/b$ . This is a symmetry of the vacuum if  $\tilde{\phi}_z$  is periodic with period length  $\ell = |\delta z|/\nu$  where  $\nu$  is integer. According to the numerical results  $\nu = 1$  at the energy minimum. Similar periodic structure is found in Wigner-crystals [14] of itinerant electrons, in certain spin systems [16] and in the charge density wave states [17]. The periodicity usually gives way to homogeneity when the external charge density is increased because the overlap integrals between the neighbouring lattice sites increase. This is not what happens in the massive Schwinger model where simple, leading order perturbation expansion shows that the ground state keeps its periodicity for arbitrarily large charge densities (see Appendix A1).

Summary: According to the tree-level approximation of the bosonized theory the massive Schwinger model has a single periodic phase in the thermodynamic limit and the homogeneous external charge density is neutralized in average by a periodic, induced charge density. Integer charges are completely screened as argued in [4].

### III. VARIATIONAL MINIMIZATION OF THE ENERGY FOR QED<sub>1+1</sub>

Let us consider now the massive Schwinger model in terms of the original fermionic degrees of freedom and subject to periodic boundary conditions at the endpoints of a finite spatial interval. The finite charge density is now introduced by the chemical potential  $\mu$ . The gas of electrons is easier to polarize than the 'empty' vacuum and accordingly there is no gap in the free electron excitation spectrum for  $\mu > m$ . The photon polarization tensor is non-vanishing at the Fermi level therefore the Debye screening renders the photon propagator short ranged and the Coulomb potential vanishing for large separation [18]. Our computation performed in this formalism supports the results obtained in the bosonized theory, namely that even an arbitrarily weak interaction among the electrons is sufficient to form a periodic ground state. The dynamical origin of the modulated ground state is the opening of a gap around the Fermi level.

We are confronted by two complications in describing the vacuum. First, the confinement of charge renders the fermionic excitation spectrum non-physical and ill-defined. As discussed above in the framework of the bosonized theory integer multiples of the elementary charge are screened by vacuum polarization at finite charge densities and their Green function is short ranged. Since only integer charges can be created in the fermionic theory we expect no problems with perturbation expansion at finite density. The second problem, the possibility of dynamical generation of coherent photons, i.e. a background field in the vacuum is more difficult and has to be handled in a self-consistent manner. For this end we introduce an external photon field,

$$\bar{A}^\nu(x^1) = \delta_0^\nu a \cos(Qx^1), \quad (15)$$

with  $a \geq 0$  chosen to be a single plane wave for the sake of simplicity. Since there is only one non-vanishing component of the field strength tensor  $F_{\mu\nu} = \partial_\mu A_\nu - \partial_\nu A_\mu$ , such a background field represents a generic sinusoidal external field in  $1+1$  dimensions. The energy density will be computed in the order  $\mathcal{O}(e^4)$  in the vacuum for a given  $\mu$  and minimized with respect to the external field, the variational parameters  $a$  and  $Q$ .

The numerical minimization of the vacuum energy density with respect to the background field shows that the theory manages to lower the vacuum energy below the ‘empty’, perturbative value by opening a gap and generating a photon condensate (15) in the vacuum for small densities. For large densities the perturbative treatment of the dependence of the vacuum energy on the field (15) is reliable and yields a gap and non-vanishing amplitude  $a$  (see Appendix A). This analysis does not cover the intermediate density regime where the density is large enough to make the numerical minimization of the two-loop energy expression unreliable but small for the application of the perturbation expansion in  $a$ .

### A. Background field as collective coordinate

The background field is introduced by the collective coordinate method into the generator functional for the Green functions. The vacuum-to-vacuum amplitude of the model is expressed by the path integral

$$Z = \int \mathcal{D}[\bar{\psi}] \mathcal{D}[\psi] \mathcal{D}[A] e^{iS_{\text{EM}}[A] + iS_{\text{D}}[A, \bar{\psi}, \psi]}, \quad (16)$$

where the action for the photon field  $A^\mu$  in Feynman gauge,

$$S_{\text{EM}}[A] = -\frac{1}{4} \int_x F^{\mu\nu} F_{\mu\nu} - \frac{1}{2} \int_x (\partial^\mu A_\mu)^2 = \frac{1}{2} A \cdot D^{-1} \cdot A, \quad (17)$$

is expressed in terms of the inverse of the free photon propagator

$$(D^{-1})_{xy}^{\mu\nu} = g^{\mu\nu} \square_x \delta_{x,y}, \quad (18)$$

and the Dirac action,

$$S_{\text{D}}[A, \psi, \bar{\psi}] = \bar{\psi} \cdot G^{-1}(A) \cdot \psi, \quad (19)$$

is given by means of the inverse fermion propagator

$$G^{-1}(A) = i\gamma^\mu (\partial_\mu - ieA_\mu) - m = \gamma^0 i\partial_0 - H_D(A) \quad (20)$$

with the Dirac-Hamiltonian

$$H_D(A) = \gamma^0 (-i\gamma^1 \partial_1 + m - e\gamma^\mu A_{x\mu}). \quad (21)$$

We use the notation  $\int_x = \int_0^T dx^0 \int_0^L dx^1$ ,  $f \cdot g = \int_x f_x g_x$  and shall consider the limit  $LT \rightarrow \infty$  below.

The vacuum of the model will be constructed by means of a variational method. We introduce an external background field  $\bar{A}_x^\nu$  and separate the quantum fluctuations  $\alpha_x^\nu$ ,  $A_x^\nu = \bar{A}_x^\nu + \alpha_x^\nu$ . The dependence on the external field is retained by the method of collective coordinates which implies the insertion of the identity

$$1 = \int d\sigma \delta(C[\bar{A}, \alpha] + \sigma) \quad (22)$$

into the path integral,

$$Z = \int d\sigma Z_\sigma, \quad Z_\sigma = \int \mathcal{D}[\bar{\psi}] \mathcal{D}[\psi] \mathcal{D}[\alpha] \delta(C[\bar{A}, \alpha] + \sigma) e^{iS_{\text{EM}}[\bar{A} + \alpha] + iS_{\text{D}}[\bar{A} + \alpha, \bar{\psi}, \psi]} \quad (23)$$

with

$$C[\bar{A}, \alpha] = \frac{1}{4} (\bar{F} - \bar{F}) \cdot \bar{F} = \frac{1}{2} \alpha \cdot D^{-1} \cdot \bar{A}. \quad (24)$$

The fluctuations of the collective coordinate  $\sigma$  are suppressed in the thermodynamic limit because the background field is extended and the  $\sigma$ -integration can be performed by expanding  $\ln Z_\sigma$  around its maximum. The contribution of the collective coordinate to the vacuum energy density will be negligible in the thermodynamic limit and the collective coordinate can be frozen at the maximum as far as the energy density in the vacuum is concerned.

One usually employs the effective action formalism in similar problems. There the external source, coupled linearly to the fluctuating field is supposed to stabilize the vacuum with the desired condensate. The minimization of the

effective action guarantees that the external source plays no role in the true vacuum. The complication which renders this method rather involved beyond the leading order of the loop expansion is the Legendre transformation. The procedure outlined above leads to simpler expressions in the two-loop order. Both methods are useful in the case of stable ground state only. Large amplitude fluctuations appear in the mixed phase which make the computation of the convex effective action and the taking into account the fluctuations of the collective coordinate difficult.

It will be useful to introduce the generator functional

$$Z[j, \bar{\zeta}, \zeta] = \int d\sigma Z_\sigma[j, \bar{\zeta}, \zeta],$$

$$Z_\sigma[j, \bar{\zeta}, \zeta] = \int d\lambda \int \mathcal{D}[\bar{\psi}] \mathcal{D}[\psi] \mathcal{D}[\alpha] e^{iS_{\text{EM}}[\bar{A} + \alpha] + iS_D[\bar{A} + \alpha, \bar{\psi}, \psi] + i\lambda(C[\bar{A}, \alpha] + \sigma) + ij \cdot \alpha + i\bar{\zeta} \cdot \psi + i\bar{\psi} \cdot \zeta}, \quad (25)$$

where the constraint is represented as a Fourier integral over  $\lambda$ . The generator functional can be written in the perturbation expansion as

$$Z_\sigma[j, \zeta, \bar{\zeta}] = \sum_{n=-\infty}^{\infty} \frac{1}{n!} \left( ie \int_x \frac{\delta}{\delta \zeta_\alpha^x} \gamma_{\alpha\beta}^\mu \frac{\delta}{\delta j_\mu^x} \frac{\delta}{\delta \bar{\zeta}_\beta^x} \right)^n Z_0 \sigma[j, \zeta, \bar{\zeta}], \quad (26)$$

where

$$Z_0 \sigma[j, \zeta, \bar{\zeta}] = \exp \left[ \text{Tr} \ln G^{-1}(\bar{A}) - i\bar{\zeta} \cdot G(\bar{A}) \cdot \zeta - \frac{4i}{a^2 Q^2 TL} \sigma^2 - \left( 2i + 4i \frac{\bar{A} \cdot j}{a^2 Q^2 TL} \right) \sigma \right. \\ \left. - \frac{1}{2} \text{Tr} \ln D^{-1} - \frac{1}{2} \ln \left( -\frac{Q^2}{4} \bar{A} \bar{A} \right) + \frac{i}{2} Q^2 \bar{A} \cdot \bar{A} - \frac{i}{2} j \cdot D' \cdot j \right] \quad (27)$$

with

$$D'_{xy}^{\mu\nu} = D_{xy}^{\mu\nu} - \frac{\bar{A}_y^\mu \bar{A}_x^\nu}{Q^2 \bar{A} \cdot \bar{A}}. \quad (28)$$

The photon propagator (28) tends to the free photon propagator in the thermodynamic limit when the fluctuations parallel to the background field vanish and we continue using the original photon propagator  $D$ .

## B. Energy and charge of the vacuum

It may happen that the system prefers energetically a periodic ground state rather than the normal, homogeneous one. Then it should adjust itself by building up a static, periodic electric field and the corresponding band structure with the Fermi-level placed in a forbidden band. In order to decide whether such a readjustment of the vacuum takes place one has to compare the energy densities of the homogeneous and modulated vacua. The fermion spectrum is needed for the determination of the energy and the charge. It has been calculated along with the corresponding eigenspinors by solving the Dirac equation numerically (see App. B and also App. C for a detailed discussion of the fermion spectrum). The fermion Green functions were constructed according to their Lehmann-expansion. The poles on the complex energy plane were shifted according to the rules established in [19] to take into account the chemical potential  $\mu$ .

### 1. Bare expression for the energy density

The effective Lagrangean corresponding to the action (25),

$$\mathcal{L} = -\frac{1}{4} F_{\rho\sigma} F^{\rho\sigma} + \frac{1}{2} \bar{\psi} i \gamma^\rho \partial_\rho \psi - \frac{1}{2} \partial_\rho \bar{\psi} i \gamma^\rho \psi + e \bar{\psi} \gamma^\rho A_\rho \psi - m \bar{\psi} \psi + \lambda \frac{1}{4} (F - \bar{F})_{\rho\sigma} \bar{F}^{\rho\sigma}. \quad (29)$$

yields the energy-momentum tensor,

$$T^{\mu\nu} = \frac{\partial \mathcal{L}}{\partial(\partial_\mu A^\kappa)} \partial^\nu A^\kappa - \frac{\partial \mathcal{L}}{\partial(\partial_\mu \psi)} \partial^\nu \psi + \partial^\mu \bar{\psi} \frac{\partial \mathcal{L}}{\partial(\partial_\nu \bar{\psi})} + \lambda \bar{F}^{\mu\kappa} \partial^\nu A_\kappa - g^{\mu\nu} \mathcal{L}, \quad (30)$$

which should be symmetrized by adding the divergence  $-\partial_\rho f^{\nu\rho\mu}$  of the third rank tensor

$$f^{\nu\mu\rho} = F^{\mu\rho} A^\nu + \frac{i}{8} \bar{\psi} (\gamma^\mu \gamma^\nu \gamma^\rho - \gamma^\rho \gamma^\nu \gamma^\mu) \psi, \quad (31)$$

determined by the spin density,

$$T_{\text{sym}}^{\mu\nu} = T^{\mu\nu} - \partial_\rho f^{\nu\rho\mu} = -F^{\mu\rho} F_\rho^\nu + \lambda \bar{F}^{\mu\kappa} \partial^\nu A_\kappa + \frac{i}{4} (\bar{\psi} \gamma^\mu \partial^\nu \psi + \bar{\psi} \gamma^\nu \partial^\mu \psi) - \frac{i}{4} (\partial^\nu \bar{\psi} \gamma^\mu \psi + \partial^\mu \bar{\psi} \gamma^\nu \psi) - g^{\mu\nu} \mathcal{L}. \quad (32)$$

It is easy to see that the symmetrized energy-momentum tensor is gauge invariant. The energy density operator is

$$\hat{\mathcal{E}}[A, \bar{\psi}, \psi] = \frac{1}{LT} \int_x T_{\text{sym}}^{00} = \frac{1}{LT} \int_x \left[ \frac{1}{2} (F_x^{01})^2 - \bar{\psi}_x H_D(A) \psi_x + \lambda \bar{F}^{0\kappa} \partial^0 A_\kappa - \frac{\lambda}{4} (F - \bar{F})_{\rho\sigma} \bar{F}^{\rho\sigma} \right], \quad (33)$$

where the first term on the r.h.s. is the energy density of the photons and the second one is the energy density of the Dirac-sea minus  $e\mu$  multiplied by the fermion density. The last two terms appear due to the exclusion of the fluctuations of the collective mode. One can write  $\hat{\mathcal{E}} = \hat{\mathcal{E}}_{(0)} + \hat{\mathcal{E}}_{(1)} + \hat{\mathcal{E}}_{(2)}$  with

$$\begin{aligned} \hat{\mathcal{E}}_{(0)}[\bar{A}, \bar{\psi}, \psi, \lambda] &= \frac{1}{LT} \int_x \left[ \frac{1}{2} (\bar{F}_x^{01})^2 + \lambda \bar{F}^{0\kappa} \partial^0 \bar{A}_\kappa - \bar{\psi}_x H_D(\bar{A}) \psi_x \right], \\ \hat{\mathcal{E}}_{(1)}[\bar{A}, \alpha, \bar{\psi}, \psi, \lambda] &= \frac{1}{LT} \int_x \alpha_{\mu x} \left( -g^{\mu 1} \partial_x \bar{F}_x^{01} + g^{\mu 0} \partial_x^1 \bar{F}_x^{01} + \frac{\lambda}{2} \square_x \bar{A}_x^\mu - \lambda \partial_x^0 \bar{F}_x^{0\mu} - e \bar{\psi} \gamma^\mu \psi \right), \\ \hat{\mathcal{E}}_{(2)}[\alpha] &= \frac{1}{LT} \int_x \frac{1}{2} [(g^{\mu 1} \partial^0 - g^{\mu 0} \partial^1) \alpha_{\mu x}] [(g^{\nu 1} \partial^0 - g^{\nu 0} \partial^1) \alpha_{\nu x}], \end{aligned} \quad (34)$$

where the lower indices indicate the powers of  $\alpha$ . The expectation value of the operator  $\hat{\mathcal{E}}$  in the vacuum is given as

$$\mathcal{E}[\bar{A}] = \frac{1}{Z} \int d\lambda \int \mathcal{D}[\bar{\psi}] \mathcal{D}[\psi] \mathcal{D}[\alpha] \hat{\mathcal{E}}[\bar{A} + \alpha, \bar{\psi}, \psi] e^{iS_{\text{EM}}[\bar{A} + \alpha] + iS_D[\bar{A} + \alpha, \bar{\psi}, \psi] + i\lambda(C[\bar{A}, \alpha] + \sigma)}. \quad (35)$$

We find

$$\begin{aligned} \mathcal{E}_{(0)}[\bar{A}] &= \frac{1}{4} Q^2 a^2 + \frac{1}{Z} \int_x \frac{\delta}{i\delta \zeta_\alpha^x} \hat{H}_D(\bar{A})_{\alpha\beta} \frac{\delta}{i\delta \zeta_\beta^x} Z_0|_{j=\zeta=\bar{\zeta}=0} \\ &\quad - \frac{e^2}{2Z} \int_x \frac{\delta}{i\delta \zeta_\alpha^x} \hat{H}_D(\bar{A})_{\alpha\beta} \frac{\delta}{i\delta \zeta_\beta^x} \int_{y,z} \frac{\delta}{\delta \zeta_y^y} \gamma_{\kappa\lambda}^\mu \frac{\delta}{\delta j_\mu^y} \frac{\delta}{\delta \zeta_y^y} \frac{\delta}{\delta \zeta_\lambda^z} \gamma_{\epsilon\delta}^\nu \frac{\delta}{\delta j_\nu^z} \frac{\delta}{\delta \zeta_\delta^z} Z_0|_{j=\zeta=\bar{\zeta}=0} \\ &= \frac{1}{4} Q^2 a^2 + \frac{1}{Z} \left[ \text{Diagram 1} - \frac{1}{2} \text{Diagram 2} + \text{Diagram 3} + \text{Diagram 4} + \frac{1}{2} \text{Diagram 5} - \text{Diagram 6} \right] \end{aligned} \quad (36)$$

with

$$Z_0 = \exp \left\{ -\frac{i}{2} j \cdot D \cdot j - i \bar{\zeta} \cdot G(\bar{A}) \cdot \zeta \right\}, \quad (37)$$

and  $\hat{H}_D(\bar{A})$  denoting the Dirac-Hamiltonian (21) with the field variables replaced by functional derivatives with respect to the corresponding external sources. The  $\mathcal{O}(\alpha^0)$  energy, Eq. (36), includes the energy density of the background and those of the modulated, interacting Dirac-sea. The  $\mathcal{O}(\alpha)$  energy term is the interaction energy of the current with the fluctuations of the photon field,

$$\begin{aligned} \mathcal{E}_{(1)}[\bar{A}] &= -\frac{ie^2}{Z} \int_{x,y} \frac{\delta}{i\delta \eta_\alpha^x} \gamma_{\alpha\beta}^\mu \frac{\delta}{i\delta j_\mu^x} \frac{\delta}{i\delta \bar{\eta}_\beta^x} \frac{\delta}{i\delta \eta_\alpha^y} \gamma_{\alpha\beta}^\nu \frac{\delta}{i\delta j_\nu^y} \frac{\delta}{i\delta \bar{\eta}_\beta^y} Z_0|_{j=\eta=\bar{\eta}=0} \\ &= -\frac{i}{Z} \left[ \text{Diagram 7} - \text{Diagram 8} \right]. \end{aligned} \quad (38)$$

The  $\mathcal{O}(\alpha^2)$  energy expression depends on the fluctuating field  $\alpha$  only. Since the photon propagator in the presence of the background field approaches the free propagator as  $L \rightarrow \infty$  the contribution  $\mathcal{E}_{(2)}$  cancels when the difference of the energy densities with and without the background field is considered.

The vacuum-to-vacuum amplitude up to the order  $\mathcal{O}(e^2)$ ,

$$\begin{aligned} Z &= 1 - \frac{e^2}{2} \int_{x,y} \frac{\delta}{\delta \zeta_\alpha^x} \gamma_{\alpha\beta}^\mu \frac{\delta}{\delta j_\mu^x} \frac{\delta}{\delta \zeta_\beta^x} \frac{\delta}{\delta \zeta_\epsilon^y} \gamma_{\epsilon\delta}^\nu \frac{\delta}{\delta j_\nu^y} \frac{\delta}{\delta \zeta_\delta^y} Z_0|_{j,\zeta,\bar{\zeta}=0} \\ &= 1 - \frac{1}{2} \left[ \text{Diagram 1} - \text{Diagram 2} \right], \end{aligned} \quad (39)$$

removes the disconnected components as expected and one finds

$$\mathcal{E}[\bar{A}] = \text{Diagram 3} - i \text{Diagram 4} + i \text{Diagram 5} + \text{Diagram 6} - \text{Diagram 7}. \quad (40)$$

The propagators are calculated by means of the Lehmann-representation

$$G_{xy}^{\alpha\beta} = \sum_{k_1 s_1} \int \frac{dk_0}{2\pi} e^{-ik_0(x_0-y_0)} \left[ \frac{f_\alpha^{k_1 s_1}(x) \bar{f}_\beta^{k_1 s_1}(y)}{k_0 + i\varepsilon} + \frac{g_\alpha^{k_1 s_1}(x) \bar{g}_\beta^{k_1 s_1}(y)}{k_0 - i\varepsilon} \right], \quad D_{xy}^{\mu\nu} = -g_{\mu\nu} \sum_{k_1} \int \frac{dk_0}{2\pi} \frac{1}{k^2 + i\varepsilon} e^{ik(x-y)}, \quad (41)$$

where  $f^{k_1 s_1}(x)$  and  $g^{k_1 s_1}(x)$  denote the positive and negative energy eigensolutions of the Dirac-equation (see App. B). The periodic background potential breaks the translational symmetry which manifests itself in changing momentum conservation to quasi-momentum conservation in each vertex.

## 2. UV and IR divergences

There is no need of mass and charge renormalizations in QED<sub>1+1</sub> and the only UV divergent diagram occurs in Eq. (40). It represents the energy of the Dirac-sea in the presence of the background field,

$$\mathcal{E}_{\text{sea}}(a, Q, \mu) = \frac{1}{TL} \text{Diagram 8} = \frac{1}{TL} \int dx \gamma_{\alpha\beta}^0 \hat{H}_D^{x(\beta)}(\bar{A}) i G_{xx}^{\beta\alpha} = -\frac{1}{TL} \sum_{k_1 s_1} \epsilon_{k_1 s_1}^{(-)}, \quad (42)$$

and is quadratically divergent in the absence of the background field,

$$\mathcal{E}_{\text{sea}}(0, 0, 0) = - \int_{-\Lambda}^{\Lambda} \frac{dp}{2\pi} [p^2 + m^2]^{1/2}. \quad (43)$$

The finite, physical part of  $\mathcal{E}_{\text{sea}}$  will be defined by

$$\mathcal{E}_{\text{per}}^{(1-l)}(a, Q, \mu) = \mathcal{E}_{\text{sea}}(a, Q, \mu) - \mathcal{E}_{\text{sea}}(0, 0, 0), \quad \mathcal{E}_{\text{n}}^{(1-l)}(\mu) = \mathcal{E}_{\text{sea}}(0, 0, \mu) - \mathcal{E}_{\text{sea}}(0, 0, 0) \quad (44)$$

for the periodic and the homogeneous, normal phases, respectively.

The convergence of  $\mathcal{E}_{\text{per}}$  was checked numerically in the following manner. The one-loop contributions are obtained by taking  $\mathcal{E}$  of Eq. (42) for the background field and subtracting from it the same diagram without background field. Let us consider first this difference for vanishing chemical potential  $\mu = 0$ ,

$$\mathcal{E}_{\text{per}}^{(1-l)}(a, Q, 0) = -\frac{1}{TL} \sum_{k_1 s_1} [\epsilon_{k_1 s_1}^{(-)}(a, Q, 0) - \epsilon_{k_1 s_1}^{(-)}(0, 0, 0)]. \quad (45)$$

By the one-by-one identification of the corresponding levels we found numerically that the magnitude  $|\epsilon_{k_1 s_1}(a, Q, 0) - \epsilon_{k_1 s_1}(0, 0, 0)|$  is suppressed for increasing  $k_1$  according to the power law

$$|\epsilon_{k_1 s_1}^{(-)}(a, Q, 0) - \epsilon_{k_1 s_1}^{(-)}(0, 0, 0)| \approx k_1^{-(1+\delta)} \quad (46)$$

with  $\delta \approx 2 > 0$ , cf. Fig. 6. This renders the sum absolutely convergent. The shift in the spectrum caused by the non-vanishing chemical potential does not alter the UV behaviour of the sum even in the thermodynamic limit. The convergence of  $\mathcal{E}_n(\mu) = \mathcal{E}(0, 0, \mu) - \mathcal{E}(0, 0, 0)$  has been checked similarly.

IR divergences can also appear at the tadpoles where the photon line carries vanishing momentum  $q^\mu = 0$ . Since there is actually no dynamical photon-field variable with vanishing energy and momenta, such tadpoles pose no problem in the homogeneous, normal vacuum [20–22]. In the periodic vacuum the photon can borrow the momentum  $nQ$  from the vacuum by the summation for  $n \neq 0$  and the tadpoles are finite.

Finally we introduce the Casimir-energy which is usually the energy difference of the states with and without a classical object and was investigated thoroughly [23] by the collective coordinate method. In our case it is the background field which plays the role of the classical object and the Casimir-energy is

$$\mathcal{E}_C(a, \mu) = \mathcal{E}_{\text{per}}(a, Q, \mu) - \mathcal{E}_n(0, 0, \mu). \quad (47)$$

### 3. Charge density

In order to understand the structure of the vacuum, we need another important observable, the average charge density  $\rho$  given as the two-loop order expectation value of the operator

$$\hat{\rho} = \frac{1}{LT} \int_x \bar{\psi} \gamma^0 \psi. \quad (48)$$

The expectation value is taken as in Eq. (35) for the energy-momentum tensor,

$$\rho[\bar{A}] = \frac{1}{LTZ} \int d\lambda \int \mathcal{D}[\bar{\psi}] \mathcal{D}[\psi] \mathcal{D}[\alpha] \psi^\dagger \psi e^{iS_{\text{EM}}[\bar{A} + \alpha] + iS_D[\bar{A} + \alpha, \bar{\psi}, \psi] + i\lambda(C[\bar{A}, \alpha] + \sigma)}. \quad (49)$$

The truncation at the two-loop order gives

$$\rho[\bar{A}] = \text{Diagram 1} + \text{Diagram 2} - \text{Diagram 3}. \quad (50)$$

These diagrams are similar to the first, fourth and fifth ones of Eq. (40) except that the Hamiltonian-insertion is replaced by a  $\gamma^0$ -insertion. Charge neutrality for  $\mu = 0$  implies the renormalization condition  $\rho_{\text{ren}}[\bar{A} \equiv 0] = 0$  which can be satisfied by the subtraction

$$\rho_{\text{ren}}[\bar{A}] = \rho[\bar{A}] - \rho[0]. \quad (51)$$

This renormalization prescription removes the UV divergence of the first diagram in Eq. (50), too. The second diagram gives vanishing contribution for vanishing periodic background electric field due to Furry's theorem. The calculations of these diagrams proceed like those for the Casimir-energy density.

## C. Results

The energy densities given by Eqs. (40) and (47) have been calculated for both phases using the explicit formulae of App. D in units of  $e = 1$ . The one-particle energy levels and spinors needed for the calculation were determined by solving numerically the system of linear equations (B4) and the sum over the components of the Bloch-waves was truncated for  $|n| \leq 25$ . This procedure provided us 50 one-particle energy levels and spinors for each momentum in the first Brillouin zone. It was tested on the fermion spectrum without background field that such a truncation starts to cause noticeable error on the spectrum for the band index  $s \approx n$  when the bands are numerated in energetically increasing order. Therefore, bands with  $s \leq 20$  have been taken into account in the calculations of the two-loop diagrams. Such a truncation allowed us to detect the effects of the background field with sufficient accuracy because it was found that for  $ea \leq m$  the distortion of the dispersion relation due to the background field is only significant for states belonging to the bands in the vicinity of  $m$ . For about 5 bands away from  $m$  the deviation of the energy levels with and without the periodic background field turns practically to zero. The one- and two-loop diagrams of Eq. (40) were computed in the first Brillouin zone  $k_1 \in [-Q/2, Q/2]$  at 40 and 10 points, respectively. The calculation

of the one-loop diagram required higher numerical accuracy due to the numerical elimination of the UV divergence. We also made a test calculation for 20 division points which corresponded to a larger volume  $L$  and found that the numerical accuracy is about 10% for the two-loop contribution to the Casimir-energy density in the whole range of the parameter values.

The amplitude  $a$  was chosen through several orders of magnitude from  $ea = 10^{-4}$  corresponding to the perturbative regime to  $ae \approx m$  for which pair-production might occur. The wavenumber of the background field was restricted to be  $Q = 0.8, 1, 1.5$  in the computation. The significantly smaller values are uninteresting from the point of view of the periodic state since the electrons become well localized in the limit  $1/Q \rightarrow \infty$  and it would cost too much energy to delocalize them. The other limit  $1/Q \rightarrow 0$  is computationally time-consuming since one has to take more Brillouin-zones into account. Therefore the summations over the band index  $s$ , as well as over the one-particle state's index  $n$  have to be truncated at increasingly higher values in the formulae of App. D. Consequences of this very restricted search of the minimum of the Casimir-energy density not allowing for the higher values  $Q > 1.5$  make our numerical results unreliable for large densities. The calculations were performed on an AlphaServer DS20 500 MHz with 2 CPU-s. In particular, it took about 2 CPU hours on a single processor to compute the diagrams in Eq. (40) for a given set of parameters  $(ea, e\mu/m, m)$  for  $Q = 0.8$ . For any given set of  $(Q, ea, m)$  we chose 50 values for  $0.5 \leq e\mu/m \leq 2$  in such a manner that the points between 0.98 and 1.35 were separated by 0.01. For  $m = 1$  we took  $a = 0.0001, 0.001, 0.01, 0.1, 0.2, 0.5, 1.0$  and  $Q = 0.8, 1.0, 1.5$ . For  $m = 0.2, 0.5, 2.0$  and 5.0 we took only the 4 larger values of  $a$ .

The negative value of the Casimir-energy indicates that the periodic state is energetically favoured. The one- and two-loop contributions to the energy are shown in Fig. 7. The one-loop contribution, i.e. that of the first diagram on the r.h.s. of Eq. (40) is more important than the two-loop terms. The two-loop correction which is dominated by the exchange diagrams, the third and the fifth ones on the r.h.s of Eq. (40), tends to destabilize the periodic state for  $e\mu < m$  and to stabilize it for  $e\mu > m$ . The periodic phase is stable mainly due to the gain arising from the sinking of upper bands to negative energies and this gain is taken into account completely in our computation since the one-particle energy levels have been calculated non-perturbatively. The photon exchange appearing at the two-loop order becomes important in the region  $e\mu \approx m$ . The numerical results for  $e\mu/m \gtrsim 1.12$  agree for the periodic and the homogeneous ground states within the numerical accuracy.

The computation of the charge density yields the equation of state, the relation between the energy and the charge density. For each  $\mu$  and  $m$  we looked for the values of  $a(\mu)$  and  $Q(\mu)$  at which the Casimir-energy density assumes its minimum. In this way we obtained  $\mathcal{E}_C(a(\mu), Q(\mu), \mu) = \mathcal{E}_C(\mu)$ , and  $\rho_{\text{ren}}(\mu)$  for each fixed value of  $m$ . The equation of state then can be constructed by tracing  $\mathcal{E}_{\text{per}}(\mu)$  and  $\mathcal{E}_n(\mu)$  as the function of  $\rho_{\text{ren}}(\mu)$  for the modulated and the homogeneous phases, respectively. A typical  $\rho$ -dependence is shown in Fig. 8 for  $m = 2$ , similar curves are found for the other values  $m$ . Two-loop calculations showed up the energy minimum for the periodic ground state for small values of  $\rho \in [0, 0.33]$  reliably, finding  $\mathcal{E}_{\text{per}}$  definitely smaller than  $\mathcal{E}_n$  (Fig. 8a). In Fig. 8b one can see that the amplitude of the static periodic background field tends to zero with increasing  $\rho$ . For densities larger than the 'critical densities'  $\rho > 0.33$  we found no energy difference between the periodic and the normal ground state within our numerical accuracy. The reliable numerical determination of the parameters  $a$  and  $Q$  became impossible, so that those are not shown in Figs. 8b, c for large densities.

The result obtained in the framework of the bosonized model, namely the small but non-vanishing amplitude of the modulation of the vacuum for large densities as shown in Fig. 5, requires special care in the numerical work. The 'critical density' above which the numerical minimization fails to find modulation, c.f. Fig. 8b, should not be considered as a phase transition, it reflects rather the insufficiency of the expected form of the induced field in the vacuum. The smallness of the amplitude of the induced field in the vacuum enables us to treat the periodic potential as perturbation at large densities. The analytic calculation of the one-loop Casimir-energy density performed in App. A 2 reveals that the ground state keeps its periodicity, although with decreasing amplitude  $a \sim \rho e^{-2\pi^3 \rho^2/e^2}$  for increasing charge density  $\rho$ . The one-loop level vacuum for the assumed simple sinusoidal background potential involves a single band sunk into the Dirac sea.

Our numerical results for  $\rho \lesssim 0.33$  show rapid oscillations in Figs. 8b and c reflecting a numerical problem that arises from our finding that the periodic states with  $Q = k_F$  and  $2k_F$  are almost degenerate. The proper treatment of this region would require more values of  $a$  and  $Q$  in the numerical computation. We found numerically that the wavenumber  $Q$  of the periodic phase is directly related to the Fermi momentum  $k_F$  via the relation  $fQ = 2k_F$ , with the filling factor  $f$ , defined as the number of the entirely filled positive-energy bands plus the fraction of the partially filled band, see Fig. 9. This relation is the consequence of the position of the Fermi-level in a forbidden zone. The product  $fQ$  is shown as the function of the charge density in Fig. 8c, it increases in the average with increasing charge density, implying the same behaviour of the wavelength as was indeed found in the bosonized theory, c.f. Fig. 4. The ratio  $Q/k_F$  displays a discrete behaviour,  $Q/k_F \approx 2$  for  $e\mu < m$  and  $Q/k_F \approx 1$  for  $e\mu > m$ . This is in agreement with the nesting relation  $fQ = 2k_F$ . The discrete nature of  $Q/k_F$  reveals that the vacuum always readjusts itself until a

forbidden zone is opened at the Fermi-level and the filling factor becomes integer. For the low-density periodic phase  $e\mu \approx m$  where the amplitude  $a$  is non-perturbative the photon exchange is significant. As  $\rho$  increases the perturbative region of  $a$  is reached, although we could not decide, whether the numerically found ‘critical density’ does fall into the perturbative region. Our one-loop perturbative result cannot clarify whether higher-order loop corrections can lead to sinking more and more bands into the Dirac sea as the density  $\rho$  increases. The one-loop estimate of the wavenumber,  $Q = 2\pi\rho$  implies that the wavelength  $2\pi/Q$  in the fermionic model also tends to zero as  $\rho$  increases, like our finding in the framework of the bosonized model (see Fig. 4).

#### IV. SUMMARY

The ground state for the massive Schwinger model has been investigated in the presence of homogeneous external charge density. The energy density of the ground state has been determined numerically in the bosonized version of the model as well as in terms of the original degrees of freedom of QED by variational methods. The scalar field configuration and the charge density of the ground state for the bosonized model have been obtained by minimizing the tree-level energy in the presence of static, homogeneous external charge density. In the fermionic theory a variational method has been constructed by minimizing for the amplitude and the wavelength of a sinusoidal photon condensate in the vacuum. The finite charge density was realized by the introduction of the chemical potential. The applicability of the loop-expansion for the computation of the vacuum energy at finite density is justified by the bosonized theory which indicates that the confining Coulomb-force among integer charges is vanishing.

The computation in the bosonized theory shows that the system exhibits a periodic ground state for arbitrary charge density. The fermionic computation gives the same result. Numerical computations reliable up to a certain charge density were completed by simple analytic calculations also supporting the periodicity of the ground state for asymptotically large charge densities. The general trends in the charge-density dependence of the amplitude and that of the wavelength of the periodic structure are in agreement for both versions of the model.

The investigations in terms of the bosonic and fermionic degrees of freedom complete one another. On the one hand, our results for the bosonized model showed that the background charge density is in average neutralized in the ground state. Furthermore, the charge density wave ground state and the complete screening of the integer charges appear due to the periodic non-linearity of the classical field equation for the boson field. The fermionic description, on the other hand, gives more insight into the structure of the vacuum, namely that the modulation of the charge density arises as the result of the opening of a gap in the fermion spectrum. The conclusion of the straightforward perturbation expansion for large charge densities is that the periodic ground state is always favoured by the system energetically as compared to the homogeneous one, even if only a single band sinks into the Dirac sea. In the case of a single mode periodic potential  $N$  bands sink below the Fermi-level in the  $N$ -th order of the perturbation expansion. In particular, in our numerical computation where a single mode was allowed for the induced photon field in the vacuum and first (second) order perturbation expression for the vacuum energy was minimized one (two) bands are found below the Fermi-level for large densities. The Peierls-mechanism is present in the relativistic vacuum for  $N \geq 2$ . It is however not clear how to identify this mechanism in terms of the bosonic excitations.

Our analytic considerations showing the existence of the periodic ground state for arbitrarily large charge densities do not include the corresponding higher-order loop corrections neither for the bosonized model, nor for the fermionic one. It still remains an open question whether a complete resummation of these higher-order corrections would alter the qualitative result obtained here, namely that the massive Schwinger model has only a single phase, the periodic one for any values of the average charge density.

#### ACKNOWLEDGEMENTS

This work has been supported by the grants OTKA T032501/00, NATO SA(PST.CLG 975722)5066, and also partially by the grant OTKA M041537 and the Supercomputing Laboratory of the Faculty of Natural Sciences, University of Debrecen. One of us (K.S.) has been supported by the Alexander von Humboldt-Foundation and he thanks W. Greiner for the kind hospitality and the impetus given by him to study strongly interacting vacua and also thanks J. Csikai making him aware of Ref. [24] in the general physics lectures nearly three decades ago.

- [1] J. Schwinger, Phys. Rev. **125**, 397, (1962); ibid. Phys. Rev. **128**, 2425, (1962)
- [2] S. Coleman, R. Jackiw, L. Susskind, Annals of Physics **93**, 267, (1975)
- [3] H. J. Rothe, K. D. Rothe, J. A. Swieca, Phys. Rev. D**19**, 3020, (1979)
- [4] W. Fischler, J. Kogut, L. Susskind Phys. Rev. D**19**, 1188, (1979)
- [5] J. Schwinger, Phys. Rev. **82**, 664, (1951)
- [6] B. E. Baaquie, J. Phys G: Nucl. Phys. **8**, 1621, (1982)
- [7] S. Coleman Phys. Rev. D**11**, 2088, (1975)
- [8] J. H. Lowenstein, J. A. Swieca, Annals of Physics **68**, 172, (1971)
- [9] S. Coleman, Annals of Physics **101**, 239, (1976)
- [10] A. Casher, J. Kogut, L. Susskind, Phys. Rev. D**10**, 732, (1976)
- [11] J. Kijowski, [arXiv:hep-th/9710003]
- [12] Y.-C. Kao, Y.-W. Lee, Phys. Rev. D**50**, 1165, (1994)
- [13] H. R. Christiansen, F. A. Schaposnik, Phys. Rev. D**53**, 3260, (1996)
- [14] E. P. Wigner, Phys. Rev. **46**, 1002, (1934)
- [15] R. E. Peierls, *Quantum Theory of Solids* (Clarendon Press, Oxford, 1955)
- [16] J. Hubbard, Phys. Rev. B**17**, 494, (1978)
- [17] G. Grüner, *Density Waves in Solids* (Addison Wesley, New York, 1994); G. Grüner and A. Zettl, Phys. Rep. **119**, 117, (1985)
- [18] S. Nagy, J. Polonyi, K. Sailer Heavy Ion Phys., Proc. Non-Euclidean Geometry in Modern Physics, 73, (2002)
- [19] R. Anishetty, J. Phys. G **10**, 423, (1984)
- [20] J. I. Kapusta, Nucl. Phys. B**148**, 461, (1979)
- [21] T. Toimela, Int. J. Th. Phys. **24**, 901, (1985)
- [22] B. A. Freedman, L. D. McLerran, Phys. Rev. D**16** (1977) 1130; ibid., Phys. Rev. D**16**, 1147, (1977)
- [23] M. Bordag, D. Robaschik, E. Wieczorek, Ann. Phys. (N.Y.) **165**, 192, (1985), D. Robaschik, K. Scharnhorst, E. Wieczorek, Ann. Phys. (N.Y.) **174**, 401, (1987)
- [24] J. C. Slater, Phys. Rev. **87**, 807, (1952)
- [25] L. Landau, M. Lifshitz, *Course of Theoretical Phys. Vol. 9.* (Pergamon Press, Oxford, 1971)
- [26] I.S. Gradstein, I.M. Ryzhik, *Table of Integrals, Series and Products* (Academic Press, New York, 1965); William H. Press, Brian P. Flannery, Saul A. Teukolsky, William T. Vetterling *Numerical Recipes in C : The Art of Scientific Computing* (Cambridge Univ. Press. Cambridge, 1992)
- [27] Tara Prasad Das, *Relativistic Quantum Mechanics of Electrons* (Harper & Row, Publishers New York, 1973)

## APPENDIX A: LARGE CHARGE DENSITIES

In this appendix we determine the ground-state energy of both the bosonic and fermionic versions of the massive Schwinger model in the limit of asymptotically large charge densities,  $\rho \rightarrow \infty$ . It was found in the numerical solutions that the amplitude of the modulation of the ground state is smaller for larger values of  $\rho$ . This feature opens the possibility of applying the perturbation expansion in the amplitude  $A$  or  $a$  of the induced periodic field in the vacuum of the bosonic or the fermionic formulation.

### 1. Bosonized model

Based on Fig. 3 the periodic part of the scalar field will be approximated by

$$\tilde{\phi}_z = A \sin \left( \frac{2\pi}{\ell} z \right). \quad (\text{A1})$$

By inserting this expression into Eq. (9) one finds the energy density

$$\mathcal{E}(A, b) \equiv \frac{E(b)}{2L} = \frac{A^2 \pi^2}{\ell^2} + \frac{\pi}{2\ell^2} + \frac{e^2 A^2}{4\pi} - \frac{cme}{\pi^{1/2}} J_1(2\sqrt{\pi}A), \quad (\text{A2})$$

where  $J_1(x)$  is the Bessel function of the first kind. Fig. 5 shows that the amplitude  $A$  decreases with increasing charge density. Therefore it is enough to consider the expression on the right hand side of Eq. (A2) only up to the order  $\mathcal{O}(A^2)$  for large  $\rho \rightarrow \infty$ . Due to the relation

$$J_1(x) \approx \frac{x}{2} + \mathcal{O}(x^3) \quad (\text{A3})$$

valid for small  $x$  the energy density takes the form

$$\mathcal{E}(A, b) = \frac{b^2}{2} + \frac{A^2}{4} \left( 4\pi b^2 + \frac{e^2}{\pi} \right) - cmeA \quad (\text{A4})$$

having a non-trivial minimum at

$$A = \frac{2cme}{4\pi b^2 + \frac{e^2}{\pi}} > 0 \quad (\text{A5})$$

where the Casimir energy is negative,

$$\mathcal{E}(A, b) - \mathcal{E}(A = 0, b) = -\frac{(cme)^2}{4\pi b^2 + \frac{e^2}{\pi}}. \quad (\text{A6})$$

Thus one concludes that the ground state of the massive Schwinger model is periodic for large external charge densities. It is shown in Fig. 5 that the analytic result of Eq. (A5) is in good agreement with the numerical one for the charge-dependence of the amplitude  $A$ .

## 2. Fermionic model

In order to better understand the gap opening mechanism of the fermionic model at large densities, a perturbative estimate of the condensate is presented below. The external potential (15) opens a gap at  $k_F = Q/2$  and according to the leading order degenerate perturbation expansion, c.f. paragraph 55 in Ref. [25] the energy spectrum is

$$\epsilon_k^\pm = \frac{1}{2} \left[ \epsilon_k^{(0)} + \epsilon_{k-Q}^{(0)} \pm \sqrt{(\epsilon_k^{(0)} - \epsilon_{k-Q}^{(0)})^2 + 4e^2 a^2} \right], \quad (\text{A7})$$

where  $\epsilon_k^{(0)}$  refers to the unperturbed spectrum and the sign  $+$  and  $-$  stand for  $|k| > \frac{1}{2}Q$  and  $|k| < \frac{1}{2}Q$ , respectively. In general, one finds  $N$  gap in the spectrum of the  $N$ -th order perturbation expansion in the monochromatic external field.

We continue with the leading order result where one finds the Casimir-energy density

$$\mathcal{E}_a = 2 \int_0^{Q/2} \frac{dk'}{2\pi} \left[ \epsilon_{\frac{1}{2}Q-k'}^- - \epsilon_{\frac{1}{2}Q-k'}^{(0)} \right] + \frac{1}{4} a^2 Q^2 \quad (\text{A8})$$

Since  $\rho = \int_{-k_F}^{k_F} dk/2\pi = k_F/\pi$  and  $Q/2 = k_F = \pi\rho$ , we have  $\rho = Q/2\pi$  which is just a special case of the nesting relation already mentioned in Sect. III C. For large values of the chemical potential  $\mu$  we expect large values of  $k_F = Q/2 \gg m$  therefore we can set  $m = 0$ , i.e.  $\epsilon^{(0)}(k) = |k|$  and perform the integral in Eq. (A8) explicitly,

$$\mathcal{E}_a = \frac{Q^2}{8\pi} + \frac{1}{4} a^2 Q^2 - \frac{Q \sqrt{Q^2 + 4e^2 a^2}}{8\pi} - \frac{e^2 a^2}{2\pi} \operatorname{arsinh} \frac{Q}{2ea}. \quad (\text{A9})$$

The Casimir-energy density has two extrema: a saddle point at  $a = 0$  ( $\partial_a^2 \mathcal{E}_{a=0} \rightarrow -\infty$ ) and a minimum at

$$a_{\min} = \frac{Q}{2e \sinh(\frac{\pi Q^2}{2e^2})} = \frac{\pi\rho}{e \sinh(\frac{2\pi^3 \rho^2}{e^2})} > 0 \quad (\text{A10})$$

( $\partial_a^2 \mathcal{E}_{a_{\min}} > 0$ ). The latter provides the Casimir-energy density of the ground state,

$$\mathcal{E}_{a_{\min}} = \frac{Q^2}{8\pi} \left[ 1 - \sqrt{1 + \frac{4e^2 a_{\min}^2}{Q^2}} \right] = \frac{\pi\rho^2}{2} \left[ 1 - \coth \frac{2\pi^3 \rho^2}{e^2} \right] < 0. \quad (\text{A11})$$

The lesson is that the vacuum (15) with  $a \neq 0$  is always favoured at the one-loop level where only a single band sinks into the Dirac sea.

For  $\rho = 0.33$  one gets  $a_{\min} \approx 0.004$  and  $\mathcal{E}_{\text{per}} - \mathcal{E}_{\text{n}} = \mathcal{E}_{a_{\min}} \approx -10^{-5}$ , so that within our numerical accuracy it was impossible to detect the periodic ground state numerically. Furthermore we have seen for lower densities that the jump from one band to two bands in the Dirac sea is a two-loop effect caused by photon exchange. Similarly, higher-loop corrections cannot be excluded for large values of the density and a more general periodic background field. Nevertheless this simple computation indicates that the vacuum of the massive Schwinger model is periodic for large values of the charge density.

## APPENDIX B: DIRAC-EQUATION WITH SINUSOIDAL POTENTIAL

The Lehmann-representation of the non-interacting electron propagator requires the knowledge of the eigenfunctions of the Dirac-Hamiltonian (21) for the external field (15). We use the real Dirac-matrices

$$\gamma^0 = \begin{pmatrix} 1 & 0 \\ 0 & -1 \end{pmatrix}, \quad \gamma^1 = \begin{pmatrix} 0 & 1 \\ -1 & 0 \end{pmatrix}. \quad (\text{B1})$$

The eigenspinors  $f^{ks}(x)$  and  $g^{ks}(x)$  of the Dirac-Hamiltonian  $H_D(\bar{A})$  belonging to the positive and negative energy eigenvalues  $\epsilon_{ks}^{(+)} > 0$  and  $-\epsilon_{ks}^{(-)} < 0$ , respectively satisfy the equations

$$H_D(\bar{A}) f^{ks}(x) = \epsilon_{ks}^{(+)} f^{ks}(x), \quad H_D(\bar{A}) g^{ks}(x) = -\epsilon_{ks}^{(-)} g^{ks}(x), \quad (\text{B2})$$

where the quasi-momentum  $k \in [-Q/2, Q/2]$  takes values in the first Brillouin-zone. The non-negative integer  $s \geq 0$  labels the bands in increasing order in the energy. As in the non-relativistic case, the solutions of Eq. (B2) are Bloch-waves,

$$f^{ks} = \sum_{n=-\infty}^{\infty} u_n^{ks} e^{-i(\epsilon_{ks}^{(+)} x_0 - k_n x_1)}, \quad g^{ks} = \sum_{n=-\infty}^{\infty} v_n^{ks} e^{i(\epsilon_{ks}^{(-)} x_0 - k_n x_1)}, \quad (\text{B3})$$

with  $k_n = k + nQ$ . In order to find the numerical solution, one rewrites Eqs. (B2) in matrix forms for the components of the Bloch-waves, e.g. the first one of Eqs. (B2) reads as

$$\sum_{n=-\infty}^{\infty} \left[ (\epsilon_{ks} + e\mu - k_n \gamma^0 \gamma^1 - m \gamma^0) u_n^{ks} + \frac{ea}{2} (u_{n+1}^{ks} + u_{n-1}^{ks}) \right] e^{-i(\epsilon_{ks} x_0 - k_n x_1)} = 0. \quad (\text{B4})$$

The solution is found by making up a matrix from the coefficients appearing next to the Dirac-spinors  $u_n^{ks}$ . The non-relativistic treatment results in a matrix with tridiagonal structure [24], [26]. The structure of the matrix remains unchanged in the relativistic case except of the replacement of the matrix elements with  $2 \times 2$  matrices. The problem is then reduced to solve a system of a coupled set of homogeneous linear equations.

## APPENDIX C: BAND STRUCTURE

In order to understand the effects of the photon exchanges, the salient features of non-interacting electrons in static periodic background field are briefly summarized in this section. The eigenspinors and the energy eigenvalues of the Dirac Hamiltonian (21) in the static, periodic external field have been determined numerically (App. B). The positive and negative single-particle energies are denoted by  $\epsilon_{ks}^{(+)}$  and  $-\epsilon_{ks}^{(-)}$ , respectively, as the functions of the quasi-momentum  $k$  and the band index  $s$ . Their dependences on the parameters  $a, Q$  are not indicated explicitly. Since the chemical potential  $\mu$  results in a constant shift of the whole fermion spectrum, it is sufficient to understand the spectrum for  $\mu = 0$ . Due to the periodic potential, a band structure with alternating allowed and forbidden bands is formed [27]. The typical band structure is plotted in Fig. 10a and 10b as the function of  $1/Q$  for undercritical  $ea < m$  and overcritical  $ea > m$  static periodic electric fields, respectively. The shaded regions in Figs. 10 correspond to the allowed bands. The non-relativistic analogue of these figures can be found in [24] where the one-dimensional electron system was considered in the presence of the static external electric potential  $A_0 = a(1 - \cos Qx)$  (with our notations) that is just the same potential we have but one of its minima is shifted to  $x = 0$  and the potential is chosen zero in this minimum. The following qualitative features of the fermion spectrum should be noted.

1. For undercritical fields  $ea < m$  the mass gap around zero energy separates the infinite towers of bands above and below this gap. The smaller is  $1/Q$ , the more the allowed bands widen out and start to overlap. This is just the qualitative behaviour obtained in the non-relativistic description [24]. The energies of the states in the upper,  $\epsilon > 0$  (lower,  $\epsilon < 0$ ) tower decrease (increase) with increasing  $1/Q$ .
2. For overcritical fields  $ea > m$  the qualitative features described above remain the same but the upper and the lower bands overlap for large enough  $1/Q$  and upper bands sink into the Dirac sea while lower bands emerge. The band crossing can well be understood [18], but this case involving creation of electron-positron pairs turned out uninteresting for our purpose, since the periodic ground state was found undercritical.

The clarifying the spectrum for the asymptotic values  $1/Q \rightarrow 0$  and  $1/Q \rightarrow \infty$  helps the understanding of the  $1/Q$ -dependence of the band structure.

1. When  $1/Q \rightarrow 0$ , the energy levels loose all information about the periodic potential and the free fermion spectrum reappears with the only gap for  $-m < \epsilon < m$ . One can easily understand this by noticing that the potential term in the Dirac Hamiltonian (21) becomes negligible compared to the kinetic energy for  $Q \rightarrow \infty$ . In fact, the introduction of the rescaled coordinate  $\xi_1 = Qx_1$  leaves the only  $Q$ -dependence coming from the gradient term of the Hamiltonian. This corresponds to infinitely densely packed atoms in the model of Ref. [24] and to vanishing average electric potential.
2. When  $1/Q \rightarrow \infty$ , the extrema of the potential become well-separated. Therefore, one expects almost localized states at the minima (maxima) corresponding to the upper (lower) bands and the reduction of each band to a single energy level which corresponds to the localized states at the various minima (maxima) of the external potential. The semiclassical tunneling probability from a minimum to the neighbouring one is suppressed exponentially with increasing  $1/Q$ ,  $w \sim \exp\{-16\sqrt{m\epsilon}/Q\}$  and the problem reduces to that of the relativistic harmonic oscillator as far as the lowest (highest) lying states of the upper (lower) band are concerned [18].

The dispersion relations in the allowed bands alternate between convex and concave ones from band to band. If the Fermi-level lies inside of an allowed band, the occupied states build either a Fermi sphere or a Fermi hole in momentum space. For one spatial dimension the Fermi sphere is distorted to a Fermi section  $p_1 \in [-k_F, k_F]$ , the Fermi hole appears as the unoccupied interval  $p_1 \in [-k_F, k_F]$  between the occupied ones,  $p_1 \in [-Q/2, -k_F]$  and  $p_1 \in [k_F, Q/2]$ .

#### APPENDIX D: TWO-LOOP DIAGRAMS FOR THE ENERGY DENSITY

Here, the explicit expressions are listed for the two-loop diagrams on the r.h.s. of Eq. (40). The eigenspinors  $u$  and  $v$  are defined in Eq. (B3). The diagrams containing tadpoles are:

$$\text{Diagram: } \textcircled{1} \text{ (tadpole)} = -ie^2 \int_{x,y} iD_{\nu\mu}^{yx} \gamma_{\alpha\beta}^\nu iG_{\beta\alpha}^{xx} \gamma_{\epsilon\delta}^\mu iG_{\delta\epsilon}^{yy} \\ = e^2 \sum_{q_1} \frac{1}{|q_1|^2} \sum_{\substack{k_1, s_1 \\ n_1, n_2}} \bar{v}_{\alpha n_1}^{k_1 s_1} \gamma_{\alpha\beta}^\mu v_{\beta n_2}^{k_1 s_1} \delta(q_1 + (n_1 - n_2)Q) \sum_{\substack{k_1, s_1 \\ n_1, n_2}} \bar{v}_{\epsilon n_1}^{k_1 s_1} \gamma_{\epsilon\delta}^\mu v_{\delta n_2}^{k_1 s_1} \delta(-q_1 + (n_1 - n_2)Q), \quad (D1)$$

$$\text{Diagram: } \textcircled{2} \text{ (tadpole)} = e^2 \int_{x,y,z} \hat{H}_D^{x(\beta)} iD_{\mu\nu}^{zy} \gamma_{\alpha\beta}^0 iG_{\beta\kappa}^{xy} \gamma_{\kappa\lambda}^\mu iG_{\lambda\alpha}^{yx} \gamma_{\epsilon\delta}^\nu iG_{\delta\epsilon}^{zz} \\ = e^2 \sum_{q_1} \frac{1}{|q_1|^2} \sum_{\substack{k_1, s_1 \\ n_1, n_2}} \bar{v}_{\epsilon n_1}^{k_1 s_1} \gamma_{\epsilon\delta}^\mu v_{\delta n_2}^{k_1 s_1} \delta_{q_1 - Q(n_1 - n_2)} \\ \times \left\{ \sum_{\substack{k_1, p_1 \\ s_1, s_2}} \frac{\sum_{n_1, n_2} \bar{u}_{\kappa n_1}^{k_1 s_1} \gamma_{\kappa\lambda}^\mu v_{\lambda n_2}^{p_1 s_2} \delta_{p_{n_2} + k_{n_1} - q_1} \sum_{n_1, n_2} \bar{v}_{\alpha n_1}^{p_1 s_2} \gamma_{\alpha\beta}^0 u_{\beta n_2}^{k_1 s_1} \epsilon_{k_1 s_1}^{(+)} \delta_{p_{n_1} + k_{n_2}}}{\epsilon_{p_1 s_2}^{(-)} + \epsilon_{k_1 s_1}^{(+)}} \right. \\ \left. - \sum_{\substack{k_1, p_1 \\ s_1, s_2}} \frac{\sum_{n_1, n_2} \bar{v}_{\kappa n_1}^{k_1 s_1} \gamma_{\kappa\lambda}^\mu u_{\lambda n_2}^{p_1 s_2} \delta_{p_{n_2} + k_{n_1} + q_1} \sum_{n_1, n_2} \bar{u}_{\alpha n_1}^{p_1 s_2} \gamma_{\alpha\beta}^0 v_{\beta n_2}^{k_1 s_1} \epsilon_{k_1 s_1}^{(-)} \delta_{p_{n_1} + k_{n_2}}}{\epsilon_{p_1 s_2}^{(+)} + \epsilon_{k_1 s_1}^{(-)}} \right\}. \quad (D2)$$

The exchange diagrams are given as

$$\text{Diagram: } \textcircled{3} \text{ (exchange)} = ie^2 \gamma_{\alpha\beta}^\nu \gamma_{\kappa\lambda}^\mu \int dx \int dy iG_{xy}^{\beta\kappa} iG_{yx}^{\lambda\alpha} iD_{y\kappa}^{\mu\nu}$$

$$\begin{aligned}
&= \frac{e^2}{2} \sum_{k_1 p_1 q_1} \sum_{n_1 n_2} \left[ \frac{\bar{v}_{\alpha n_4}^{p_1 s_2} \gamma_{\alpha \beta}^{\mu} u_{\beta n_1}^{k_1 s_1} \delta_{k_1, n_1 + p_1, n_4 + q_1} \bar{u}_{\kappa n_2}^{k_1 s_1} \gamma_{\kappa \lambda}^{\mu} v_{\lambda n_3}^{p_1 s_2} \delta_{k_1, n_2 + p_1, n_3 + q_1}}{|q_1| (|q_1| + \epsilon_{k_1 s_1}^{(+)} + \epsilon_{p_1 s_2}^{(-)})} \right. \\
&\quad \left. + \frac{\bar{u}_{\alpha n_4}^{p_1 s_2} \gamma_{\alpha \beta}^{\mu} v_{\beta n_1}^{k_1 s_1} \delta_{k_1, n_1 + p_1, n_4 - q_1} \bar{v}_{\kappa n_2}^{k_1 s_1} \gamma_{\mu \kappa \lambda} u_{\lambda n_3}^{p_1 s_2} \delta_{k_1, n_2 + p_1, n_3 - q_1}}{|q_1| (|q_1| + \epsilon_{k_1 s_1}^{(-)} + \epsilon_{p_1 s_2}^{(+)})} \right], \tag{D3}
\end{aligned}$$

$$\begin{aligned}
&\text{Diagram: A circle with a wavy line inside, labeled 'H' at the top. Arrows indicate a clockwise flow around the circle.} \\
&= -\frac{e^2}{2} \int_{x,y,z} \gamma_{\alpha \beta}^0 \gamma_{\epsilon \delta}^{\mu} \gamma_{\kappa \lambda}^{\nu} \hat{H}_{D,x}^{(\beta)}(\bar{A}) (\mathrm{i} D_{yz}^{\mu \nu} \mathrm{i} G_{zy}^{\lambda \epsilon} \mathrm{i} G_{xz}^{\beta \kappa} \mathrm{i} G_{yx}^{\delta \alpha}) \\
&= \frac{e^2}{4} \sum_{\substack{k_1 p_1 r_1 q_1 \\ s_1 s_2 s_3}} \frac{1}{|q_1|} \\
&\quad \left[ \frac{\sum_{n_1 n_2} \bar{u}_{n_1}^{k_1 s_1} \gamma_{\mu} v_{n_2}^{r_1 s_3} \delta_{k_1, n_1 + r_1, n_2 + q_1} \sum_{n_1 n_2} \bar{u}_{n_1}^{p_1 s_2} \gamma^{\mu} u_{n_2}^{k_1 s_1} \delta_{k_1, n_2 - p_1, n_1 + q_1}}{(|q_1| + \epsilon_{k_1 s_1}^{(+)} + \epsilon_{r_1 s_3}^{(-)}) (\epsilon_{p_1 s_2}^{(+)} + \epsilon_{r_1 s_3}^{(-)})} \right. \\
&\quad \sum_{n_1 n_2} \bar{v}_{n_1}^{r_1 s_3} \gamma^0 u_{n_2}^{p_1 s_2} [\epsilon_{p_1 s_2}^{(+)} \delta_{p_1, n_2 + r_1, n_1}] + \\
&\quad \sum_{n_1 n_2} \bar{u}_{n_1}^{k_1 s_1} \gamma_{\mu} u_{n_2}^{r_1 s_3} \delta_{k_1, n_1 - r_1, n_2 + q_1} \sum_{n_1 n_2} \bar{v}_{n_1}^{p_1 s_2} \gamma^{\mu} u_{n_2}^{k_1 s_1} \delta_{k_1, n_2 + p_1, n_1 + q_1} \\
&\quad \left. \frac{(|q_1| + \epsilon_{k_1 s_1}^{(+)} + \epsilon_{p_1 s_2}^{(-)}) (\epsilon_{p_1 s_2}^{(-)} + \epsilon_{r_1 s_3}^{(+)})}{(|q_1| + \epsilon_{k_1 s_1}^{(+)} + \epsilon_{p_1 s_2}^{(-)}) (|q_1| + \epsilon_{k_1 s_1}^{(+)} + \epsilon_{r_1 s_3}^{(-)})} \right. \\
&\quad \sum_{n_1 n_2} \bar{u}_{n_1}^{r_1 s_3} \gamma^0 v_{n_2}^{p_1 s_2} [-\epsilon_{p_1 s_2}^{(-)} \delta_{p_1, n_2 + r_1, n_1}] - \\
&\quad \sum_{n_1 n_2} \bar{u}_{n_1}^{k_1 s_1} \gamma_{\mu} v_{n_2}^{r_1 s_3} \delta_{k_1, n_1 + r_1, n_2 + q_1} \sum_{n_1 n_2} \bar{u}_{n_1}^{p_1 s_2} \gamma^{\mu} u_{n_2}^{k_1 s_1} \delta_{k_1, n_2 + p_1, n_1 + q_1} \\
&\quad \left. \frac{(|q_1| + \epsilon_{k_1 s_1}^{(+)} + \epsilon_{p_1 s_2}^{(-)}) (|q_1| + \epsilon_{k_1 s_1}^{(+)} + \epsilon_{r_1 s_3}^{(-)})}{(|q_1| + \epsilon_{k_1 s_1}^{(-)} + \epsilon_{p_1 s_2}^{(+)}) (|q_1| + \epsilon_{k_1 s_1}^{(-)} + \epsilon_{r_1 s_3}^{(+)})} \right. \\
&\quad \sum_{n_1 n_2} \bar{v}_{n_1}^{r_1 s_3} \gamma^0 v_{n_2}^{p_1 s_2} [-\epsilon_{p_1 s_2}^{(-)} \delta_{p_1, n_2 - r_1, n_1}] + \\
&\quad \sum_{n_1 n_2} \bar{u}_{n_1}^{k_1 s_1} \gamma_{\mu} u_{n_2}^{r_1 s_3} \delta_{k_1, n_1 + r_1, n_2 - q_1} \sum_{n_1 n_2} \bar{u}_{n_1}^{p_1 s_2} \gamma^{\mu} v_{n_2}^{k_1 s_1} \delta_{k_1, n_2 + p_1, n_1 - q_1} \\
&\quad \left. \frac{(|q_1| + \epsilon_{k_1 s_1}^{(-)} + \epsilon_{p_1 s_2}^{(+)}) (|q_1| + \epsilon_{k_1 s_1}^{(-)} + \epsilon_{r_1 s_3}^{(+)})}{(|q_1| + \epsilon_{k_1 s_1}^{(-)} + \epsilon_{r_1 s_3}^{(+)}) (|q_1| + \epsilon_{k_1 s_1}^{(-)} + \epsilon_{p_1 s_2}^{(+)})} \right. \\
&\quad \sum_{n_1 n_2} \bar{u}_{n_1}^{r_1 s_3} \gamma^0 v_{n_2}^{p_1 s_2} [-\epsilon_{p_1 s_2}^{(-)} \delta_{p_1, n_2 + r_1, n_1}] - \\
&\quad \sum_{n_1 n_2} \bar{u}_{n_1}^{k_1 s_1} \gamma_{\mu} v_{n_2}^{r_1 s_3} \delta_{k_1, n_1 - r_1, n_2 - q_1} \sum_{n_1 n_2} \bar{u}_{n_1}^{p_1 s_2} \gamma^{\mu} v_{n_2}^{k_1 s_1} \delta_{k_1, n_2 + p_1, n_1 - q_1} \\
&\quad \left. \frac{(|q_1| + \epsilon_{k_1 s_1}^{(-)} + \epsilon_{p_1 s_2}^{(+)}) (\epsilon_{p_1 s_2}^{(+)} + \epsilon_{r_1 s_3}^{(-)})}{(|q_1| + \epsilon_{k_1 s_1}^{(-)} + \epsilon_{p_1 s_2}^{(+)}) (\epsilon_{p_1 s_2}^{(+)} + \epsilon_{r_1 s_3}^{(-)})} \right. \\
&\quad \sum_{n_1 n_2} \bar{v}_{n_1}^{r_1 s_3} \gamma^0 v_{n_2}^{p_1 s_2} [\epsilon_{p_1 s_2}^{(+)} \delta_{p_1, n_2 + r_1, n_1}] \Big]. \tag{D4}
\end{aligned}$$

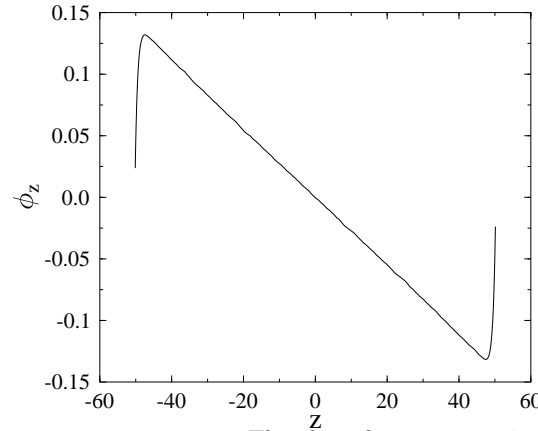


FIG. 1. The scalar field  $\phi_z$  for  $b = 0.025$ ,  $m = e = 1$ . The slope  $b_s = -0.001078$  fitted in the central region should be compared to  $b_s = be^2/(\kappa^2\pi) = -0.001074$  from Eq. (14).

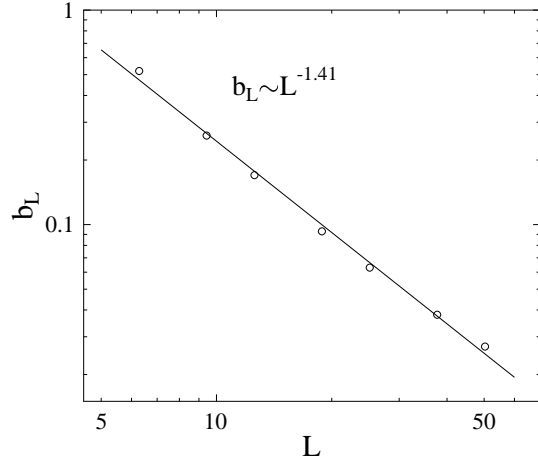


FIG. 2. Dependence of the point  $b_L$  on the size  $L$  of the system for  $m = e = 1$ .

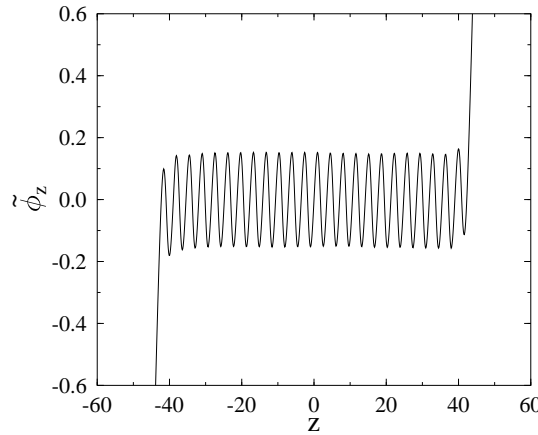


FIG. 3. The periodic part  $\tilde{\phi}_z$  of the scalar ground-state field configuration for  $b = 0.5$ ,  $m = e = 1$ .

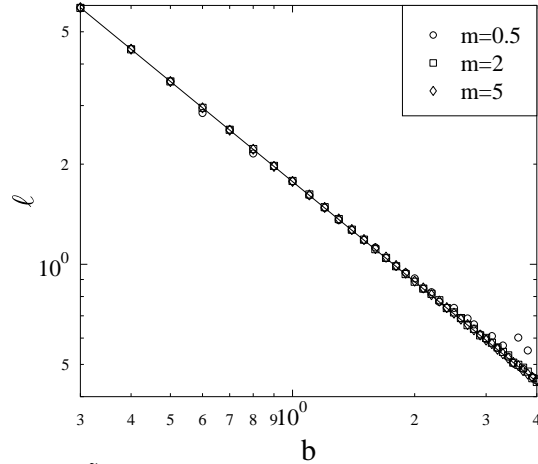


FIG. 4. Wavelength  $\ell$  of the periodic part  $\tilde{\phi}_z$  vs. the parameter  $b$  for various values of the electron mass  $m$  and  $e = 1$ . The solid line refers to the curve  $\ell = \sqrt{\pi}/b \equiv 1/\rho_{\text{ext}}$ .

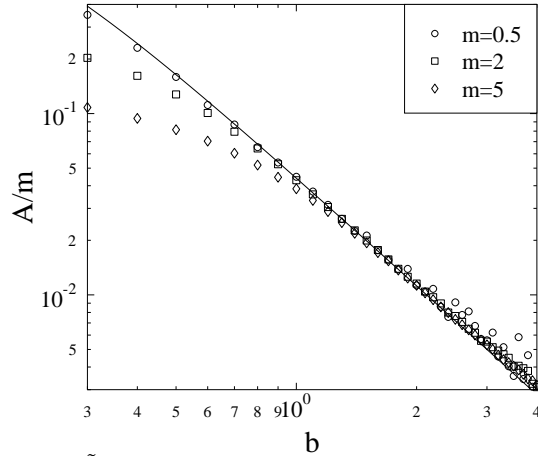


FIG. 5. Amplitude  $A$  of the periodic part  $\tilde{\phi}_z$  vs. the parameter  $b$  for various values of the electron mass  $m$  and  $e = 1$ . The solid line represents our perturbative estimate for the amplitude given by Eq. (A5) in App.A. The numerical values justify the perturbative estimate for small values of  $A$ .

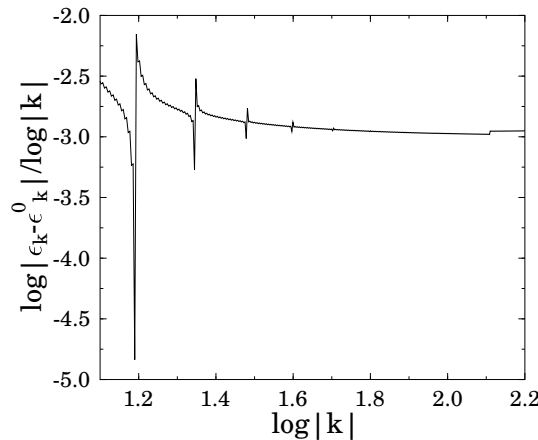


FIG. 6. Momentum-dependence of the difference of the single particle energies in the expression (45) of the one-loop energy for  $m = 2$ ,  $Q = 1.1$  and  $a = 2$ .

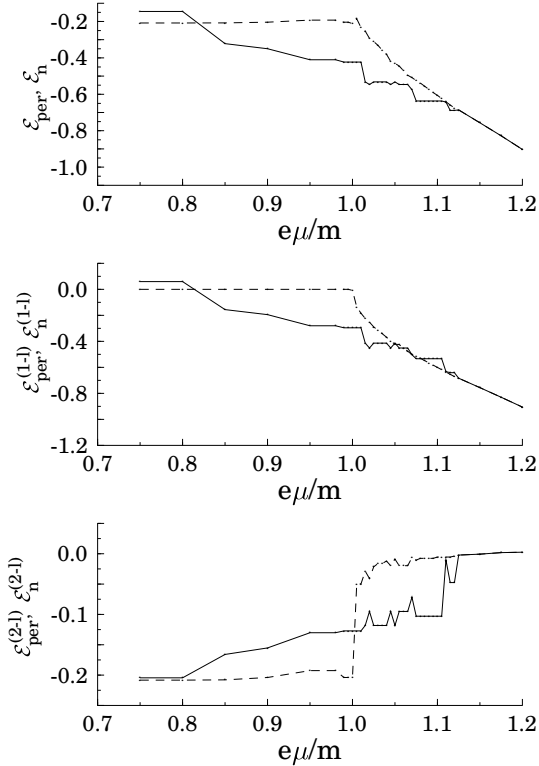


FIG. 7. (a) Energy densities vs.  $e\mu/m$  (up), and (b) the one-loop (middle) and (c) two-loop (down) contributions to those. The solid and dashed lines refer to the periodic and the homogeneous phases, respectively.

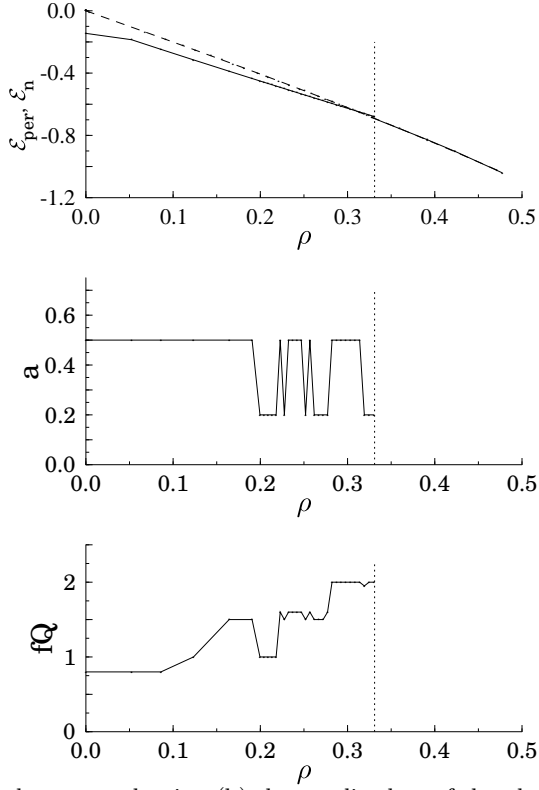


FIG. 8. Density dependences of (a) the energy density, (b) the amplitude  $a$  of the photon condensate and (c) the product of the filling factor  $f$  and the wavenumber  $Q$  of the photon condensate for  $m = 2$ . The dotted lines indicate the ‘critical charge density’  $\rho_c$ , solid and dashed lines correspond to the periodic and normal phases, respectively.

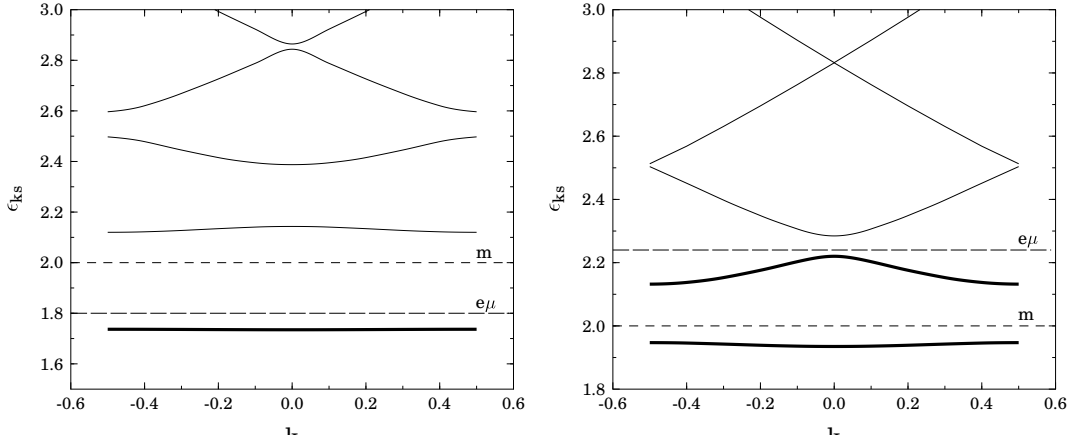


FIG. 9. Dispersion relations in the first Brillouin-zone with (a) one occupied band (left) and (b) two occupied bands (right) sunk into the Dirac sea for  $ea = 0.5$  and  $ea = 0.2$ , respectively,  $m = 2$ .

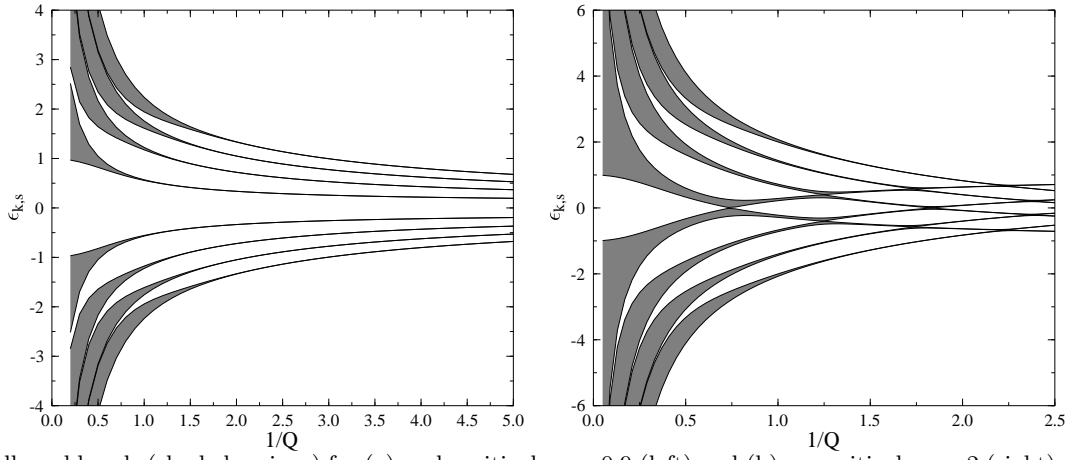


FIG. 10. Allowed bands (shaded regions) for (a) undercritical  $ea = 0.9$  (left) and (b) overcritical  $ea = 2$  (right) static periodic external fields with wavenumber  $Q$  for  $m = e = 1$ .